Original Research

Synergism of arsenic trioxide and MG132 in Raji cells attained by targeting BNIP3, autophagy, and mitochondria with low doses of valproic acid and vincristine

Victoria Cavaliere [b,3], Tomás Lombardo [a,2], Susana N. Costantino [b], Laura Kornblihtt [c], Elida M. Alvarez [b,1], Guillermo A. Blanco [a,1,*]

[a] *Laboratorio de Immunotoxicologia (LaITo), IDEHU-CONICET, Hospital de Clínicas, José de San Martín, Universidad de Buenos Aires (UBA), Buenos Aires, Argentina*
[b] *Laboratorio de Inmunología Tumoral (LIT), IDEHU-CONICET, Facultad de Farmacia y Bioquímica, UBA, Buenos Aires, Argentina*
[c] *Servicio de Hematología, Hospital de Clínicas, José de San Martín (UBA), Buenos Aires, Argentina*

Abstract   We previously demonstrated that arsenic trioxide (ATO) and proteasome inhibitor MG132 synergistically induced cell death in promonocytic leukaemia cell line U937 but were antagonistic in Burkitt's lymphoma cell line Raji. Here we explore the role of autophagy, expression of BNIP3, and mitochondrial mass, in determining whether ATO and MG132 interaction can be shifted from antagonism to synergism in Raji cells. Treatment with ATO + MG132 increased the percentage of cells with collapsed mitochondrial membrane potential (MMP) in U937 cells, but had no effect in Raji cells. Mitochondria were found in cytoplasmic marginal location in U937 cells but at perinuclear location in Raji cells. ATO + MG132 increased mitochondrial mass in U937 cells but decreased it in Raji cells, while autophagy was increased in both cell lines. BNIP3 was expressed in U937 cells at cytoplasmic marginal locations and was hardly detected in Raji cells. Histone deacetylase (HDAC) inhibitor valproic acid (VPA) increased expression of BNIP3 in Raji cells at perinuclear locations. However antagonism between ATO and MG132 was increased in the presence of low doses of VPA. Addition of vincristine (VCR) blocked autophagy, while VPA + VCR treatment of Raji cells at sub-cytotoxic doses caused BNIP3 and mitochondria to redistribute to cytoplasmic peripheral location and increased mitochondrial mass. ATO + MG132 in the presence of subcytotoxic doses of VPA + VCR caused collapse of MMP in Raji cells, while

 * *Corresponding author at:* Laboratorio de Inmunotoxicología (LaITo), IDEHU-CONICET – UBA, Junin 956 4to piso, Capital Federal 1113, Argentina. Tel.: +54 11 4964 8259x123; fax: +54 11 4964 0024.
    E-mail address: gblanco@ffyb.uba.ar (G.A. Blanco).
[1] Member of the National Research Career (CONICET).
[2] Fellow from UBA.
[3] Fellow from CONICET.

interaction between ATO and MG132 shifted from antagonism to synergism. We conclude that synergism between ATO and MG132 was attained in Raji cells by disruption of the perinuclear mitochondrial cluster, blockage of selective autophagy of mitochondria (mitophagy) by VCR, increased mitochondrial mass, and upregulation of BNIP3 by VPA.

1. Introduction

Arsenic trioxide (ATO) is in clinical use for newly diagnosed promyelocytic leukaemia (PML) achieving high efficacy and minimal toxicity in long-term follow-up [1,2]. The mechanism of ATO-induced cell death is not completely understood but appears to involve mitochondrial disruption, increased production of reactive oxygen species (ROS), and triggering of intrinsic apoptosis [3,4]. ATO was shown to target and eliminate leukaemia initiating stem cells in mouse models via PML targeting [5]. However the single-agent clinical activity of ATO in other haematological malignancies has been limited by the high doses required to induce cell death. Combination of ATO with other targeted drugs such as the proteasome inhibitors may sensitise malignant cells and lower the ATO doses required to achieve cell death [6].

The Chou–Talalay combination index (CI) method provides a valuable assessment of cytotoxic drug interaction since it can describe whether a combination of drugs is synergic (CI < 1), additive (CI = 1) or antagonistic (CI > 1) over an entire range of cytotoxic effects [7,8]. By using the CI method we have previously demonstrated that ATO combined with the proteasome inhibitor MG132 are synergic in the promonocytic leukaemia cell line U937 and antagonistic in Burkitt's lymphoma cell line Raji [9]. It is useful to bring together results of cytotoxic drug interaction studies with known mechanistic models because the latter provide a rationale to target cell death resistance and the former may conclude on the pharmacological relevance of the targeted mechanism, particularly if antagonism is turned into synergism. In the present study we explored the potential influence of mechanistic models of cell death already described by other authors, with the aim of targeting these mechanisms, overcoming resistance and changing the kind of interaction between ATO and MG132 in Raji cells from antagonism (CI > 1) to synergism (CI < 1). In particular, we explored a drug resistant system that appears to involve the formation of perinuclear mitochondrial clusters [10], the elimination of mitochondria, and the expression of the Bcl2-family member protein BNIP3, all of which may be targeted to modify the effect of cytotoxic drugs [11–13]. BNIP3 is a member of the Bcl2 family of proteins with a role in response of normal cells to hypoxia [11,14]. Its role in cancer cells remains controversial since several studies have demonstrated that overexpression of BNIP3 induces cell death, while many others demonstrated a pro-survival role [11,12,14,15]. BNIP3 was shown to provide survival advantage in cancer cells by promoting mitochondrial autophagy and eliminating damaged mitochondria with low membrane potential as a source of intracellular ROS [11,16,17]. This mechanism would allow cancer cells to neglect cell death signals induced by drugs that target the mitochondria [11,12,14]. In cells having a prominent role of this system mitochondria and BNIP3 may be localised in proximity to the nucleus [10,18]. Formation of perinuclear mitochondrial clusters requires a functional microtubule network and may be disrupted by microtubule inhibitors [12,19,20]. Despite its role in this pro-survival mechanism, BNIP3 was found to mediate hypoxia-induced cell death [21,22], and arsenic-induced cell death in tumour cells [23]. Moreover, silencing of the BNIP3 gene by epigenetic mechanisms was shown to protect cancer cells from hypoxia or drug-induced cell death; and BNIP3 was proposed as a molecular target for treating a subset of haematopoietic tumours through activation of apoptosis by methyltransferases and histone deacetylase (HDAC) inhibitors [11,24]. Thus, paradoxically BNIP3 appears to have a dual role either promoting cell survival or inducing cell death depending on the particular tumour or cell type, but it is not completely understood what factors determine whether it has a pro-survival or a pro-death role [11,14]. In the present study we explored the expression of BNIP3 in U937 and Raji cells and we evaluated the role of epigenetic drugs in sensitising Raji cells to the combination of ATO + MG132. We brought up the hypothesis that antagonism between MG132 and ATO in Raji cells (CI > 1) could be reverted to synergism (CI < 1) by desilencing BNIP3 with epigenetic drugs. However the sole expression of BNIP3 would not result in synergism if it happened to be expressed with a pro-survival role. Thus, our hypothesis included an additional contribution of the perinuclear mitochondrial cluster and mitochondrial autophagy to the alleged pro-survival role of BNIP3. We therefore explored the possibility of blocking any survival role of BNIP3 by introducing low doses of the microtubule inhibitor vincristine (VCR).

We found that shifting of antagonism to synergism between ATO and MG132 in Raji cells was associated with both upregulation of BNIP3 by low doses of the HDAC inhibitor valproic acid (VPA) and disruption of the perinuclear mitochondrial clusters by VCR.

2. Materials and methods

2.1. Reagents, cell lines and culture conditions

ATO was a kind gift from Varifarma (Argentina). Fresh stock solutions of 1 mM ATO were prepared before every experiment. 5-azacytidine (Mielozitidina) was kindly provided by Laboratorio LKM (Argentina). MG-132 was obtained from Calbiochem (San Diego, CA, United States of America (USA)), and stock solutions were prepared in dimethylsulphoxide (DMSO) at 5 mM stock concentration. Valproic acid was from Casasco Pharmaceuticals (Argentina) and was prepared freshly as a 100 mM stock solution in RPMI-1640 medium. Vincristine was kindly provided by Laboratorio Filaxis (Argentina). RPMI-1640, penicillin, streptomycin, fluorescein-diacetate (FDA), tetramethylrhodamine-ethyl-ester (TMRE), propidium iodide (PI), monodansylcadaverine (MDC), Nonyl-acridine orange (NAO), MitoTrackerR Red (MTKred), and 4′,6-diamidino-2-phenylindole (DAPI) were purchased from Invitrogen (Buenos Aires, Argentina). U937 cells were purchased from ECACC and Raji cells were purchased from ATCC. Both cell lines were grown in RPMI 1640 with 10% heat-inactivated foetal calf serum, at 37 °C in a 5% CO_2 atmosphere. Cells were subcultured at 1:2 ratios every 2–3 days with a viability greater than 95% (assessed by trypan blue) maintaining cell concentrations between 0.5 and 1.5×10^6/ml.

2.2. Cell death and autophagy assessment through flow cytometry

U937 or Raji cells were decanted in 24-well culture plates at 0.5×10^6/ml. Serial dilutions of ATO, MG132, VPA, VCR or drug combinations were added in triplicate. RPMI was added as untreated control. All experiments to determine EC50 or CI were conducted considering dose ranges and intervals to cover the entire effect range (i.e. from no cytotoxic effect to maximal cytotoxic effect) unless otherwise indicated [8,9]. The plates were incubated for either 24 h or 72 h at 37 °C with 5% CO_2. To identify dead cells, live non-autophagic cells and live autophagic cells samples were labelled with FDA, MDC and PI. Briefly, samples were incubated at 37 °C in 1 μM FDA in RPMI for 15 min, 50 μM MDC for 10 min, washed three times in phosphate buffered saline (PBS) by centrifugation, transferred to flow cytometry tubes, stained with 1 μM PI, and immediately run in a Partec PAS III flow cytometer equipped with a 20 mW 488 argon laser and a 365 nm 100 W UV lamp excitation line (Partec, Germany). A total of 20,000 cells were analysed for each dose or time point in triplicate. The MDC, FDA and PI fluorescence were collected through a 480/15 nm, 535/15 nm and 680/15 bandpass filter respectively. Quadrant analysis was done with Flomax software (Partec, Germany).

For complementary microscopic observations, cells were stained for 10 min with 50 μM MDC but without adding FDA or PI. Samples were washed in PBS and mounted onto slides for immediate live observation under fluorescence microscopy.

2.3. Median-effect and combination index analysis of cytotoxicity

The detailed procedure of this analysis was described previously [8,9]. Briefly, for each single or combined drug treatment the fraction of dead cells Fa, and live cells $Fu = (1 - Fa)$ was determined by flow cytometry. By linear regression we obtained the slope and the intercept of the equation $\log(Fa/Fu) = m \cdot \log(D) - m \cdot \log(Dm)$ (where Dm is the median dose and D is the independent variable) to further derive the median effect formula for each drug as:

$$D = Dm(Fa/(1 - Fa))^{1/m}$$

With this formula we could further estimate the dose D that induces cytotoxicity in a fraction Fa of cells in a 72 h incubation experiment. For each level of cytotoxicity i, combination index (CI) values CI(i) were then calculated according to following equation:

$$CI(i) = Dac(i)/Das(i) + Dbc(i)/Dbs(i) + \alpha Dac(i) \cdot Dbc(i)/Das(i) \cdot Dbs(i)$$

where Dac(i) and Dbc(i) are the doses of drugs a and b respectively required in the combination a + b to produce an effect level i.

Das(i) and Dbs(i) are the doses of drug a and b, respectively, required to produce an effect level i when used as single drugs. Since we used constant molar ratios of drugs a and b in the combination assays and we assumed a conservative mutually non-exclusive interaction where $\alpha = 1$, the final formula was:

$$CI(i) = Dac(i)/Das(i) + Dac(i) \cdot R/Dbs(i) + Dac(i) \cdot R \cdot Dac(i)/Das(i)Dbs(i)$$

where R was the molar ratio of drug b to drug a in the combined drug assay. Calculations were done with the software Calcusyn (Biosoft, United Kingdom (UK)), which implements the above formulas, assisted with Microsoft Excel spreadsheets to check results, perform regression analysis and create improved graphs.

2.4. Mitochondrial membrane potential

The mitochondrial transmembrane potential was evaluated by the potentiometric probe TMRE [25]. Cells were incubated in 0.05 μM TMRE for 20 min at 37 °C. The mitochondrial uncoupling agent carbonyl cyanide 3-chlorophenylhydrazone (CCCP) (50 μM) was included as a positive control. DAPI at a 1 μg/ml final concentration was added as a membrane non-permeant

dye to label dead cells and simultaneously assess mitochondrial membrane potential (MMP) and viability [26]. Cells were washed once with PBS and 20,000 cells per sample were analysed in a PAS III flow cytometer with Blue and UV excitation lines as described above. Histogram and mean fluorescence analysis was made with Flomax software.

2.5. Light and fluorescence microscopy

In all cases the slide preparations were observed in an Olympus BX-51 fluorescence microscope equipped with a 100 Watt mercury lamp, a halogen lamp for transmitted light, U-plan fluorite objectives and three fluorescence filter cubes (U-MWU2, U-MWB2 and U-MWG2 for ultraviolet, blue and green excitation light respectively). All images were acquired with a digital Q-Color 3 Olympus camera and Image-Pro Plus 6.0 software (Media Cybernetics, USA). Image processing was performed with Image-Pro Plus 6.0. DAPI and MDC fluorescence was evaluated at excitation wavelength of 330–385 nm (U-MWU2 filter). Fluorescein (FITC) fluorescence was evaluated at excitation wavelength of 450–480 nm (U-MWB2 filter). MitoTrackerR Red (MTKred) fluorescence and RFP-LC3 fluorescence were evaluated at excitation wavelength of 510–550 nm (U-MWG2 filter).

2.6. Evaluating mitochondrial cell distribution and mitochondrial mass with MTKred and NAO

A stock solution of 1 mM MTKred was prepared in DMSO and further used to label cells by suspending them at a final concentration of 50 nM during 20 min at 37 °C in PBS, then washed once in PBS and mounted onto slides for microscopic observation. An average of 60 images of red fluorescent and phase contrast fields at $1000\times$ magnification per treatment were acquired. To compute the mitochondrial area the fluorescent MTKred image of each cell (at $1000\times$ magnification) was surrounded with a contour line (shown in Fig. 1D) with the automatic segmentation tool provided by the software Image-Pro Plus 6.0. The area was computed from pixels above a threshold fluorescence value without considering actual fluorescence intensity above the threshold value. The correct recognition for each cell was verified by direct observation before computing the mitochondrial area. The total area of the same cell was computed from the corresponding phase contrast image of the same field. Scoring was conducted at 24 h exposure in samples treated with 72 h single or combined EC50 doses where viability remained as high as untreated sample having no shrinkage or change in forward light scatter (FSC) versus side light scatter (SSC) bivariate distribution (data not shown). The area measurements were exported to Excel spreadsheets and the ratio [area of MTKred-labelled mitochondria]/[total cell area] computed for each cell was used as an indicator of the mitochondrial

distribution. Nonyl-acridine orange, a green fluorescent probe that binds to cardiolipin was used to estimate mitochondrial mass by flow cytometry. A 5 mM stock solution of NAO in ethanol was diluted to 100 nM in PBS to stain cells during 30 min at 37 °C. The cells were washed once in PBS and analysed by flow cytometry.

2.7. Immunofluorescence detection of BNIP3

Cells were fixed in 4% formaldehyde in PBS during 30 min at 4 °C. To quench autofluorescence after fixation they were suspended in 25 mM ammonium chloride in PBS. Cells were further washed and mounted onto slides, air dried and permeabilised in methanol at −20 °C during 10 min; then washed in PBS and blocked for 1 h in PBS containing 2% normal rabbit serum, 1% BSA and 0.3% Triton X-100. Preparations were washed and incubated overnight at 4 °C with mouse anti-human BNIP3 (Abcam, Cambridge, UK) diluted 1/200 in PBS with 2% BSA; then washed and incubated with FITC-conjugated secondary antibody rabbit anti-mouse IgG (Sigma, MO, USA) for 1 h at RT. Preparations were washed, stained with 1 μg/ml DAPI, and observed under a BX-51 fluorescence microscope. More than 50 images at $1000\times$ magnification were acquired with equal exposure time for each treatment (Q-Color 3 Olympus camera) to compare fluorescence intensity.

2.8. mRNA extraction and semi-quantitative reverse transcription-polymerase chain reaction (RT-PCR)

Total mRNA from samples (5×10^6 cells) was isolated with TRIZOL according to the protocol recommended by the manufacturer, and RT-PCR was conducted as described previously [27]. Negative controls for reverse transcription were (1) RNA sample subjected to RT in the absence of enzyme to control for intrinsic contamination by genomic DNA, and (2) reverse transcription performed without adding RNA to control for contamination during the experiment. Positive control included the use of RNA samples known to give positive results. cDNA was then amplified using BNIP3 sense primer 5′-CCACCTCGCTCGCAGA-CACCAC-3′ and BNIP3 antisense primer 5′-GAGA-GCAGCAGAGATGGAAGGAAAAC-3′ [24]. The thermal profile used was: denaturing at 94 °C, extension at 72 °C, annealing at 66 °C (3 cycles), 64 °C (4 cycles), 62 °C (5 cycles), 60 °C (23 cycles), with a total of 35 cycles (product size: 317 bp). To evaluate the relative expression of the BNIP3 gene, the β-actin gene was also amplified by 25 cycles (60 s at 94 °C, 60 s at 52 °C and 60 s at 72 °C) followed by a 10 min extension at 72 °C, using sense primer 5-ATGGATGACGATATCGCT-3 and antisense 5-ATGAGGTAGTCTGTCAGGT-3 (product size: 570 bp). Serial dilutions were used for each cDNA to ensure that amplification occurred within the exponential range and that the reaction did not reach
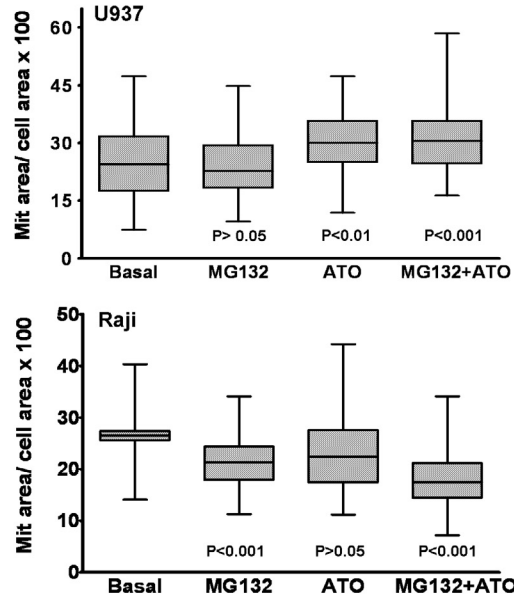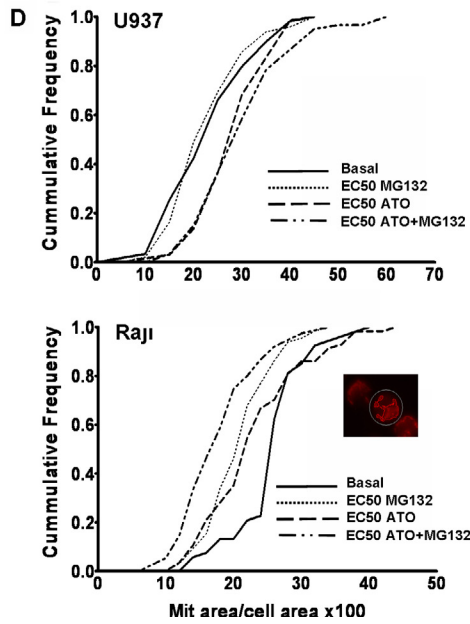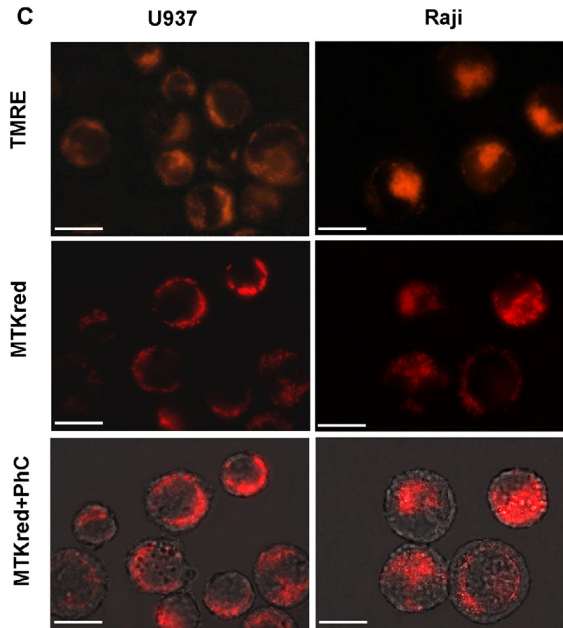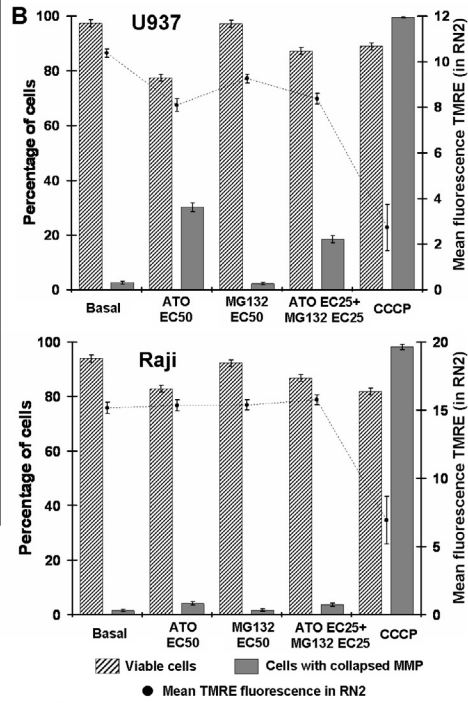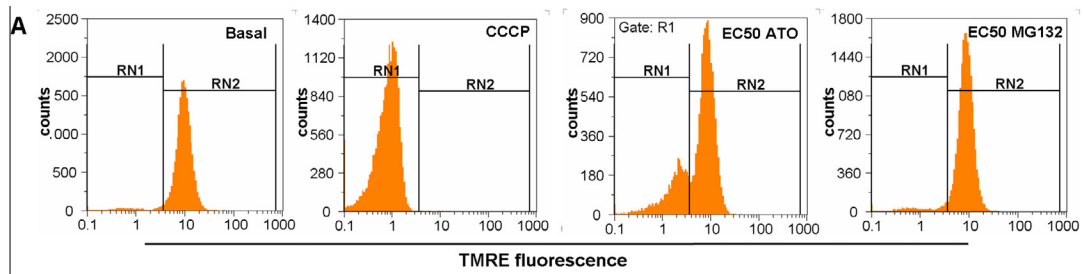
the plateau. PCR products were separated in 2.5% and 1.5% agarose gel (BNIP3 and actin respectively), stained with GelRed TM (Biotium-Hayward, USA) and visualised under UV light in a UV-transilluminator (Cole Palmer Instrumental). Gel images obtained with a digital camera (Olympus, Camedia, D-510) were subjected to densitometry analysis using Image Scion software. The relative abundance of BNIP3 gene transcripts was determined by dividing the densitometry values of the PCR product by that of β-actin.

2.9. Cytoplasmic extracts and western blot detection of BNIP3 and LC3

To prepare protein extracts 2×10^6 cells from each sample were incubated in 400 μl of hypotonic buffer (20 mM Tris pH 8.0, 150 mM NaCl, 100 mM NaF, 10% glycerol, 1% Nonidet P-40, 1 mM PMSF, 40 μg/ml leupeptin, and 20 μg/ml aprotinin) for 30 min at 4 °C. The supernatants were stored at −70 °C until further use, and protein concentration was determined by Bradford assay. Equal amounts of protein extracts (50 μg/lane) in sample buffer (2% SDS, 10% glycerol, 25 mM Tris pH 6.8, 4 M urea, 1% 2-mercapto-ethanol) were resolved by SDS–polyacrylamide gel electrophoresis (12% for BNIP3 and 15% for LC3,) and transferred onto PVDF-membranes (GE Healthcare, Argentina). The membrane was blocked overnight at 4 °C in Tris-buffered saline, containing 2% glycine and 3% non-fat dried milk. In a next step the membrane was incubated overnight at 4 °C with specific antibodies to BNIP3 (Abcam, Cambridge, UK), LC3 (Cell Signaling Technologies), or β-actin (Santa Cruz Biotechnology, CA, USA) followed by horseradish peroxidase-labelled secondary antibody for 1.5 h at 37 °C. The reaction was developed using a chemo-luminescence detection system (Luminol Reagent, Santa Cruz Biotechnology, Inc.). Densitometry analysis was carried out using Scion Image software (Scion Corporation, NIH, Bethesda, MD).

2.10. Assessment of DNA content

Raji cells were treated with a range of doses of ATO in duplicates and cultured for 72 h in RPMI 10% FBS. They were washed once in PBS and fixed in ice-cold 70% ethanol for 60 min. Then cells were washed two times in PBS and stained with 1 μg/ml PI during 30 min at RT. Cellular DNA content was measured using a PAS III flow cytometer. Twenty thousand events were acquired for each sample. Results were analysed using Flomax software. Regions corresponding to G0/G1, S and G2/M phase were determined in untreated samples with the cell cycle module of Flomax software.

2.11. Transfection of Raji cells with pRFP-LC3 and MDC colocalisation analysis

Raji cells were transfected with pRFP-LC3 using DMRIE-C transfection reagent (Invitrogen, Argentina) as indicated by the manufacturer. The transfected cells were incubated for 48 h in RPMI-1640 supplemented with 10% FBS without antibiotic in 12-well plates, and further re-suspended in RPMI 10% FBS with antibiotic and treated with 3 mM VPA or 3 mM VPA + 1 μM VCR. After 24 h cells were stained with 50 μM MDC 30 min at 37 °C, washed once in RPMI and observed by fluorescence microscopy equipped with a digital Q-Color 3 Olympus camera. A replicate sample of transfected cells was kept separately without MDC staining (Single RFP fluorescence). Another control was made with non-transfected Raji cells stained with MDC. Excitation with 330–385 nm U-MWU2 filter of these MDC single-stained cells showed no signal in the red channel. Excitation with the same UV filter of pRFP-LC3-transfected cells without MDC staining showed no signal in the blue channel. Thus no crosstalk was found between the two fluorophores. Fluorescence intensities of images remained within the response range of the microscope. Colocalisation analysis was conducted with Image-Pro

Fig. 1. Effect of 72 h cytotoxic doses of arsenic trioxide (ATO) and MG132 on the mitochondrial membrane potential (MMP) and mitochondrial mass after 24 h treatment in U937 and Raji cells. (A) Fluorescence of cells labelled with the potentiometric probe tetramethylrhodamine-ethyl-ester (TMRE) analysed through histograms to determine the percentage of cells with collapsed MMP (RN1) and the mean TMRE fluorescence of cells still having a positive MMP (cells in RN2). To set the limit between the two populations a sample was treated with the uncoupler CCCP to induce complete collapse of MMP, and the histogram obtained was compared with that of untreated cells. Histograms are depicted to illustrate how values were obtained to further produce the bar graphs shown in B. (B) MMP status of cells treated with 72 h cytotoxic doses and evaluated at 24 h (see Table 1 for the corresponding EC% doses in μg). Bar graphs show the percentage of viable cells as determined by exclusion of the non-permeable dye 4′,6-diamidino-2-phenylindole (DAPI), cells with collapsed MMP, and the mean fluorescence of cells still having a positive MMP. Samples were assayed in triplicate and error bars indicate ±SD of the mean value. (C) Dissimilar intracellular distribution of mitochondria in U937 and Raji cells. Polarised mitochondria in U937 cells labelled by TMRE were found evenly distributed in the cytoplasm, while in Raji cells polarised mitochondria were found clustered in central areas around the nucleus. The dissimilar distribution between U937 and Raji cells was confirmed with MitoTrackerR Red (MTKred), a probe that binds covalently to mitochondria and is retained even if MMP collapses. MTKred + PhC indicates a digital overlay of MTKred fluorescent image and a phase contrast image of the same field to appreciate the relative distribution of mitochondria within the cells. Size bar corresponds to 10 μm. (D) MTKred fluorescent images were used to analyse individual cells and score the area of mitochondrial fluorescence and the area of the whole cell, to further compute a ratio of these areas as an indicator of mitochondrial mass. Left graphs show the cumulative frequency distribution, and right panels the matching Box–Whisker plot and the p-values corresponding to Tukey–Kramer's post test of treatment versus basal comparison after a significant ANOVA test ($p < 0.001$). The inset shows a MTKred fluorescent image of a Raji cell surrounded with the segmentation software tool to illustrate calculation of mitochondrial area (see Section 2).

Plus 6.0 software (Media Cybernetics, USA). Blue and red channel images were processed with green and red pseudocolour respectively to produce colocalisation merge images. Correlation analysis and bidimensional scattergrams of biologically relevant regions of the samples were performed with Image Pro Plus 6.0.

2.12. Combined staining with MDC and acridine orange (AO) and colocalisation analysis

For microscopic observations of combined staining of lysosomes and autophagosomes Raji cells were stained first with 50 µM MDC in RPMI at 37 °C during 10 min. They were washed in PBS and further stained with 0.5 µM AO immediately before mounting onto slides for live observation under fluorescence microscopy. Single stained samples were used as controls to assure there was no crosstalk between the two probes.

2.13. Combined staining with MDC and MTKred and colocalisation analysis

For microscopic observations of combined staining of mitochondria and autophagosomes Raji cells were stained with MTKred as described above and were further incubated with 50 µM MDC in RPMI at 37 °C during 10 min, washed once in PBS and mounted onto slides for live observation under fluorescence microscopy. Single stained samples were used as controls to assure there was no crosstalk between the two probes.

2.14. Combined staining with MTKred and anti-BNIP3 and colocalisation analysis

For microscopic observations of combined staining of mitochondria and BNIP3 Raji or U937 cells were stained first with MTKred as described above, washed in PBS and fixed in 4% formaldehyde in PBS during 30 min at 4 °C. Permeabilisation and labelling with anti BNIP3 and FITC-conjugated antibody was conducted as described in the above section always protected from light.

2.15. Statistical analysis

Multiple comparisons were analysed by an ANOVA test using the Tukey–Kramer post test for differences between the means of treated groups with basal untreated group. Data of mitochondrial mass measurements obtained with Image-Pro Plus 6.0 were exported to and analysed with Graph-Prism 4.0 (GraphPad, San Diego, CA, USA), to further produce the cumulative distribution and Box-Whisker plots.

3. Results

3.1. Dissimilar effect of ATO and MG132 on the mitochondrial membrane potential (MMP) in U937 and Raji cells

We first assessed the effects of ATO and MG132 on the MMP in U937 and Raji cells.

We previously determined by the median effect and combination index methods the single and combined doses of ATO and MG132, required to induce cell death at 72 h to different levels [9]. Dose values used in this study with their estimated cytotoxic effect level at 72 h are presented in Table 1 together with the combination index (CI). We used these 72 h cytotoxic doses, referred herein simply as EC%, in assays conducted at 24 h to explore the differential effect on MMP between cell lines prior to the occurrence of cell death at 72 h. Calculation of EC% requires an accurate estimate of cell death to categorise single cells as dead or alive. This was

Table 1
Cytotoxic doses of arsenic trioxide (ATO) and MG132 in U937 and Raji cells.

Effect level (EC%) at 72 h	ATO (µM) ± SD	MG132 (µM) ± SD	ATO (µM) + MG132 (µM)	Combinatory index (CI) ± SD[*]
U937 cells				
EC25	3.93 ± 0.37	1.35 ± 0.08	1.82 + 0.45	0.80 ± 0.09
EC30	4.53 ± 0.38	1.50 ± 0.09	2.02 + 0.51	0.78 ± 0.08
EC40	5.84 ± 0.43	1.80 ± 0.11	2.43 + 0.61	0.75 ± 0.07
EC50	7.37 ± 0.52	2.13 ± 0.14	2.89 + 0.72	0.73 ± 0.06
EC70	11.99 ± 1.06	3.02 ± 0.23	4.12 + 1.03	0.68 ± 0.06
EC80	16.33 ± 1.80	3.78 ± 0.32	5.17 + 1.29	0.66 ± 0.06
EC90	26.00 ± 3.93	5.29 ± 0.55	7.27 + 1.82	0.62 ± 0.08
Raji cells				
EC25	6.53 ± 0.28	0.35 ± 0.04	5.90 + 0.49	5.70 ± 2.64
EC30	7.19 ± 0.29	0.50 ± 0.05	6.62 + 0.55	3.91 ± 1.37
EC40	8.50 ± 0.29	0.91 ± 0.08	8.13 + 0.68	2.26 ± 0.40
EC50	9.93 ± 0.30	1.58 ± 0.13	9.81 + 0.82	1.59 ± 0.11
EC70	13.71 ± 0.35	3.52 ± 0.60	14.52 + 1.21	1.18 ± 0.04
EC80	16.84 ± 0.44	5.92 ± 1.19	18.65 + 1.55	1.15 ± 0.05
EC90	22.95 ± 0.75	12.93 ± 3.30	27.15 + 2.26	1.19 ± 0.06

[*] The complete CI versus effect level functions with 95% confidence intervals and experimental values for U937 and Raji cells are shown in Fig. 4C and D, respectively.

accomplished by FDA/PI labelling and flow cytometry assessment. Determination of EC% is based on cell death rates and not on cell death phenotype indicators such as the fraction of cells undergoing DNA degradation. However, due to the fact that apoptosis rather than passive necrosis is observed at doses close to EC50, the rate of cells having late apoptotic phenotype can be often close to the rate of dead cells obtained with the FDA/PI method at least within a limited dose range. The amount of cells having subG1 DNA content after 72 h exposure to EC20 to EC90 ATO was compared to the amount of dead cells scored by the FDA/PI method and results are shown in Supplementary Fig. S1. Both methods were coincident around the ATO EC50 dose but not at higher doses such as EC70 or EC90 where the true fraction of dead cells was underestimated by the fraction of SubG1 cells (Supplementary Fig. S1).

ATO applied at an EC50 dose increased the percentage of U937 cells with collapsed MMP evaluated at 24 h, and lowered the MMP in those cells that still kept a positive MMP, as indicated by decrease of the mean fluorescence of TMRE (cells in RN2 region in Fig. 1A). MG132 at an EC50 dose did not change the percentage of U937 cells with collapsed MMP when evaluated at 24 h, while ATO EC25 + MG132 EC25 induced a higher percentage of cells with collapsed MMP than MG132 EC50 but less than ATO EC50 (Fig. 1B). Even though we used a 72 h EC50 dose, in most of the samples the viability at 24 h was above 80%, as indicated by the absence of DAPI fluorescence (Fig. 1B). By contrast, in Raji cells none of the treatments with ATO EC50, MG132 EC50 or ATO EC25 + MG132 EC25 induced any change in MMP, either in the percentage of cells with collapsed MMP, or the level of MMP (Fig. 1B).

In untreated U937 cells, polarised mitochondria labelled with TMRE were evenly distributed all around the cytoplasm, and the fluorescence was frequently observed close to the cell membrane limit (Fig. 1C). By contrast, in untreated Raji cells polarised mitochondria formed large clusters particularly at inner areas close to the nucleus, and were rarely seen approaching the cell membrane edge (Fig. 1C). This differential distribution of mitochondria between untreated U937 cells and Raji cells was confirmed with the use of MitoTrackerR Red (MTKred) (Fig. 1C).

When U937 cells were treated with ATO EC50 or ATO EC25 + MG132 EC25 and evaluated at 24 h, the area of fluorescent mitochondria was increased in MTKred-labelled cells, while there was no change in the cell location of fluorescence compared to untreated cells (Fig. 1C,D, and Supplementary Fig. S2). The assessment of mitochondrial mass with NAO probe by flow cytometry, which measures the amount of mitochondria regardless the polarisation state, showed an increase over basal levels with all three treatments ATO EC50,

MG132 EC50 and ATO EC25 + MG132 EC25 (Supplementary Fig. S3). In contrast, Raji cells treated with ATO EC25 + MG132 EC25 showed lower mitochondrial fluorescent area, while the fluorescence of MTKred was found close to the nucleus (Fig. 1 C,D, and Supplementary Fig. S2). In addition, MG132 EC50 significantly decreased mitochondrial fluorescent area in Raji cells compared to basal levels, but not in U937 cells (Fig. 1D). The assessment with NAO by flow cytometry showed decreased mitochondrial mass in Raji cells with all three treatments (ATO, MG132 and ATO + MG132) when compared to basal levels (Supplementary Fig. S3).

3.2. ATO and MG132 induced autophagy in Raji and U937 cells

Under specific circumstances such as hypoxia, autophagy may contribute to eliminate mitochondria with low MMP and decrease mitochondrial mass [28]. Thus we explored the presence of basal autophagy in Raji and U937 cells and the potential changes induced at 24 h by ATO EC50, MG132 EC50 and ATO EC25 + MG132 EC25. Both Raji and U937 cells showed basal autophagy as detected by the presence of LC3II by western blot (Fig. 2A). LC3II was increased after treatment with MG132 EC50, ATO EC50 and MG132 EC25 + ATO EC25 (Fig. 2A). The changes in LC3 levels after inhibition of autophagic flux are shown in Fig. S13A. The size, number, and cellular distribution of autophagosomes, as identified by MDC staining and fluorescence microscopy, were different between cell lines. Raji cells had larger dot-like autophagosome images and stronger fluorescence than U937 cells (Fig. 2B). However, there was a wide range of fluorescence intensities and dot sizes among cells, from strong fluorescence with many large dots to almost non-fluorescent cells. Thus autophagy as detected at the single cell level by this method was variable, while the western blot method showed an average measure due to the fact that the sample is reduced to a homogenate and normalised to protein content. Therefore, to further quantify changes in MDC-stained cells we used UV-excited flow cytometry as a high throughput method. We first confirmed that Rapamycin, a well known inducer of autophagy, was detected in a dose-dependent manner by this method (Fig. 2C and D). Since autophagy is considered a dynamic process where autophagosomes are continuously formed and eliminated by fusion with lysosomes, we further evaluated blockage of autophagic flux by VCR (Fig. 2D). VCR like other vinca alkaloids are known to prevent the fusion of autophagosomes with lysosomes, thus increasing the amount of MDC-stained autophagosomes in Rapamycin-treated cells after a short incubation time [29]. Changes in autophagic flux in Rapamycin-treated cells as detected by LC3 and western blot are also shown in Fig. S13B.
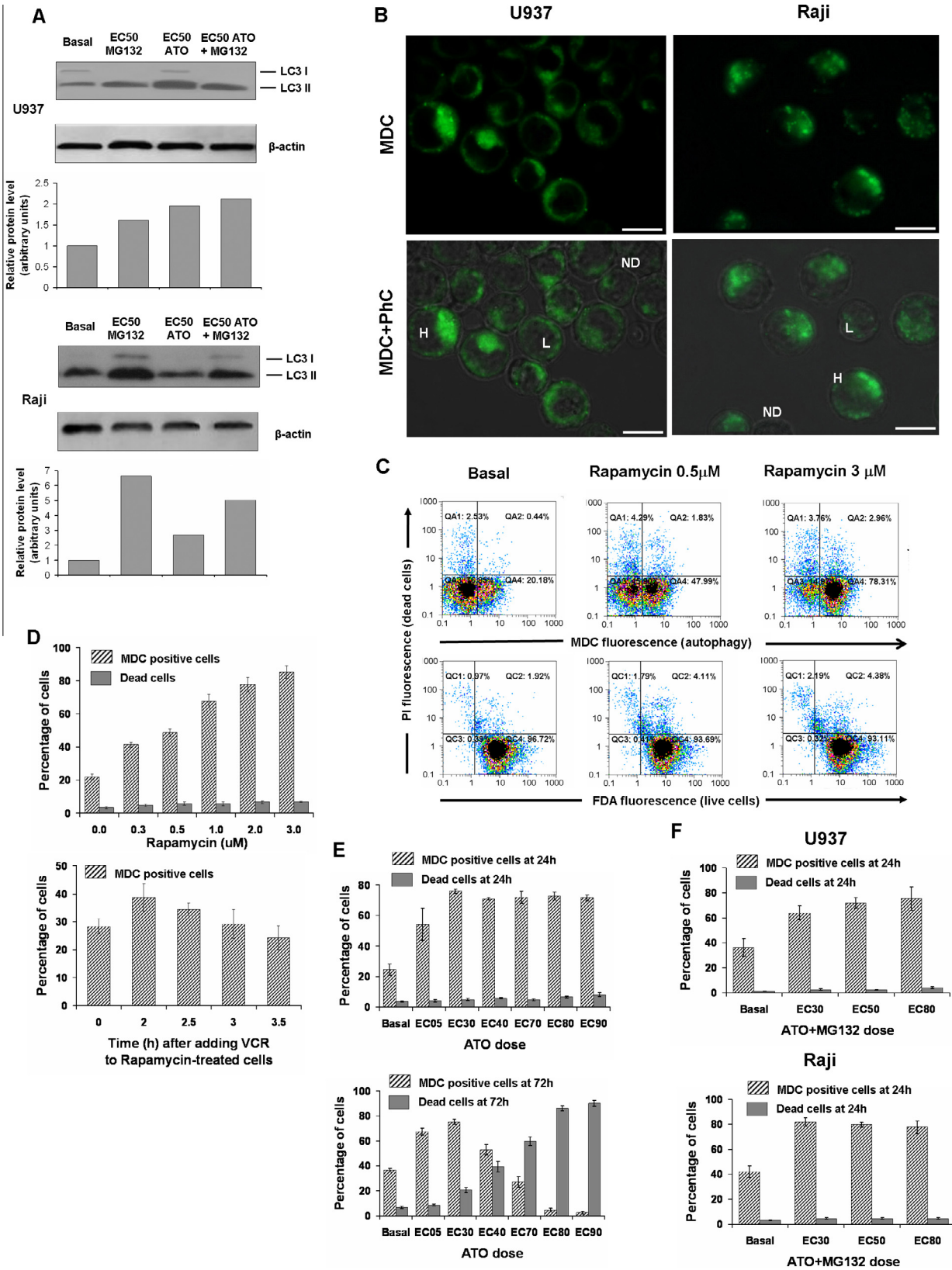
These assays proved that the percentage of cells with MDC-positive staining obtained from 20,000 scored cells in triplicate by UV excited flow cytometry was an indicator of the level of autophagy (Fig. 2D). MDC did not stain lysosomes or late acidic autophagolysosomes but only early and intermediate autophagosomes. In a combined staining with MDC and AO, a probe that stains red fluorescent acid vesicles, the majority of MDC stained vesicles and AO-stained vesicles did not colocalise (Supplementary Fig. S4).

We further confirmed by flow cytometry of MDC-labelled cells that ATO increased autophagy in Raji cells evaluated at 24 h over the range EC05 to EC90 of 72 h cytotoxic doses (Fig. 2E). However, when evaluated at 72 h, only samples treated with cytotoxic doses of ATO at EC40 or below retain autophagic levels above that of untreated cells (Fig. 2E). In fact, above the peak value observed at EC30 there was a clear inverse relationship between the EC% dose and autophagy, meaning that the more dead cells were found in the sample the less the chance that autophagy would be detected in the remaining live cells (Fig. 2E). We next confirmed that the combination ATO + MG132 increased the percentage of MDC-positive cells in Raji and U937 cells, after 24 h incubation with 72 h cytotoxic doses (EC30, EC50 and EC80). Again viability remained high at 24 h even though these doses would have caused cell death at 72 h (Fig. 2F). Thus the combination MG132 + ATO increased autophagy in both cell lines even though it proved to be synergic in U937 cells and antagonistic in Raji, ruling out the possibility that changes in autophagy levels could self explain the opposed kind of interaction that ATO and MG132 had in the two cell lines.

3.3. Differential expression of BNIP3 in U937 cells and Raji cells

BNIP3 protein was easily detected by immunofluorescence in U937 cells with an even distribution all around the cytoplasm (Fig. 3A). By contrast it was hardly detected in Raji cells since fluorescence intensity was slightly above that of negative controls (Fig. 3A). BNIP3 was also detected at the mRNA level in untreated U937 cells by conventional RT-PCR (Fig. 3B). U937 cells treated with 72 h cytotoxic doses and evaluated at 24 h showed increased BNIP3 mRNA with MG132 EC50, and a slight decrease with ATO EC50 and MG132 EC25 + ATO EC25 (Fig. 3B). Instead, BNIP3 mRNA was barely detected in Raji cells and no change was detected with MG132 EC50, ATO EC50 or MG132 EC25 + ATO EC25 (Fig. 3B).

3.4. VPA upregulated BNIP3 in Raji cells

We found a clear upregulation of BNIP3 mRNA by 1 μM 5-azacytidine (Fig. 3B). In addition, the HDAC inhibitor VPA had a similar BNIP3 mRNA upregulating effect in Raji cells at 2, 3, and 4 mM dose (Fig. 3B and Fig. S14). VPA also appeared to increase BNIP3 mRNA in U937 cells using the same dose range (Fig. 3B). Raji cells exposed to 3 mM VPA for 24 h together with MG132 at EC30, EC40 and EC50 doses showed increased BNIP3 mRNA (Fig. 3B). Raji cells treated with 3 mM VPA for 24 h also showed increased BNIP3 protein when evaluated by immunofluorescence (Fig. 3C). However, BNIP3 was found mostly with uneven cellular distribution, close to the nucleus and apart from the peripheral areas of the cytoplasm, contrasting to the uniform cytoplasmic distribution that we observed in untreated and VPA-treated U937 cells (Fig. 3C). We further confirmed that VPA increased the expression of BNIP3 in Raji cells by western blot (Fig. 3D).

We wanted to use VPA as a sensitising drug without contributing itself to cytotoxicity but to an upregulation of BNIP3 that could potentiate ATO + MG132 treatment. Therefore, we conducted cytotoxicity assays at 72 h (scored by labelling with FDA/PI and flow

Fig. 2. Basal and drug-induced autophagy in U937 and Raji cells. (A) Western blot image showing expression of LC3I and LC3II in untreated cells (basal), and cells treated with single and combined arsenic trioxide (ATO) and MG132 for 24 h with 72 h cytotoxic doses. The corresponding actin expression and results of densitometry analysis are shown below. The corresponding EC% doses expressed in μM are detailed in Table 1. (B) Untreated Raji and U937 cells stained with monodansylcadaverine (MDC). Some cells showed high fluorescent large dots (H), some other cells showed dim fluorescent small dots (L), and even other cells showed no detectable fluorescence (ND). MDC + PhC indicates digitally overlaid fluorescent and phase contrast images to appreciate the cellular distribution of autophagosomes. Size bar = 10 μm. (C) Simultaneous assessment of autophagy and cell death by flow cytometry after 24 h of Rapamycin treatment. Plots correspond to three representative samples used to produce the bar graphs shown in panels below. The quadrant analysis of MDC versus propidium iodide (PI) is shown in the top row (autophagy versus membrane damage), and that of FDA versus PI in the bottom row (live cells having metabolic activity versus membrane damage). (D) Bar graph showing the percentage of MDC positive cells (i.e. having abundant autophagosomes) among live Raji cells (PI negative) at increasing doses of Rapamycin after 24 h incubation, and percentage of dead cells (PI positive) at 24 h with increasing doses of Rapamycin. Samples were assayed in triplicate and error bars indicate ±SD of the mean value. The lower bar graph shows the percentage of MDC-positive Raji cells treated with 0.25 μM Rapamycin for 24 h, and the changes that occurred after the addition of 1 μM vincristine (VCR) to block autophagic flow. There was an early increase in autophagosomes (owing to inhibition of late fusion of autophagosomes and lysosomes) followed by a progressive time-related decrease. (E) Raji cells treated with increasing doses of ATO (EC0 to EC90) and evaluated for autophagy and cell death at 24 h (graph on top), and 72 h (graph below). The corresponding μM values of EC% doses are shown in Table 1. (F) U937 cells (graph on top) and Raji cells (graph below) treated with increasing 72 h cytotoxic doses of ATO + MG132 and evaluated at 24 h for autophagy and cell death.
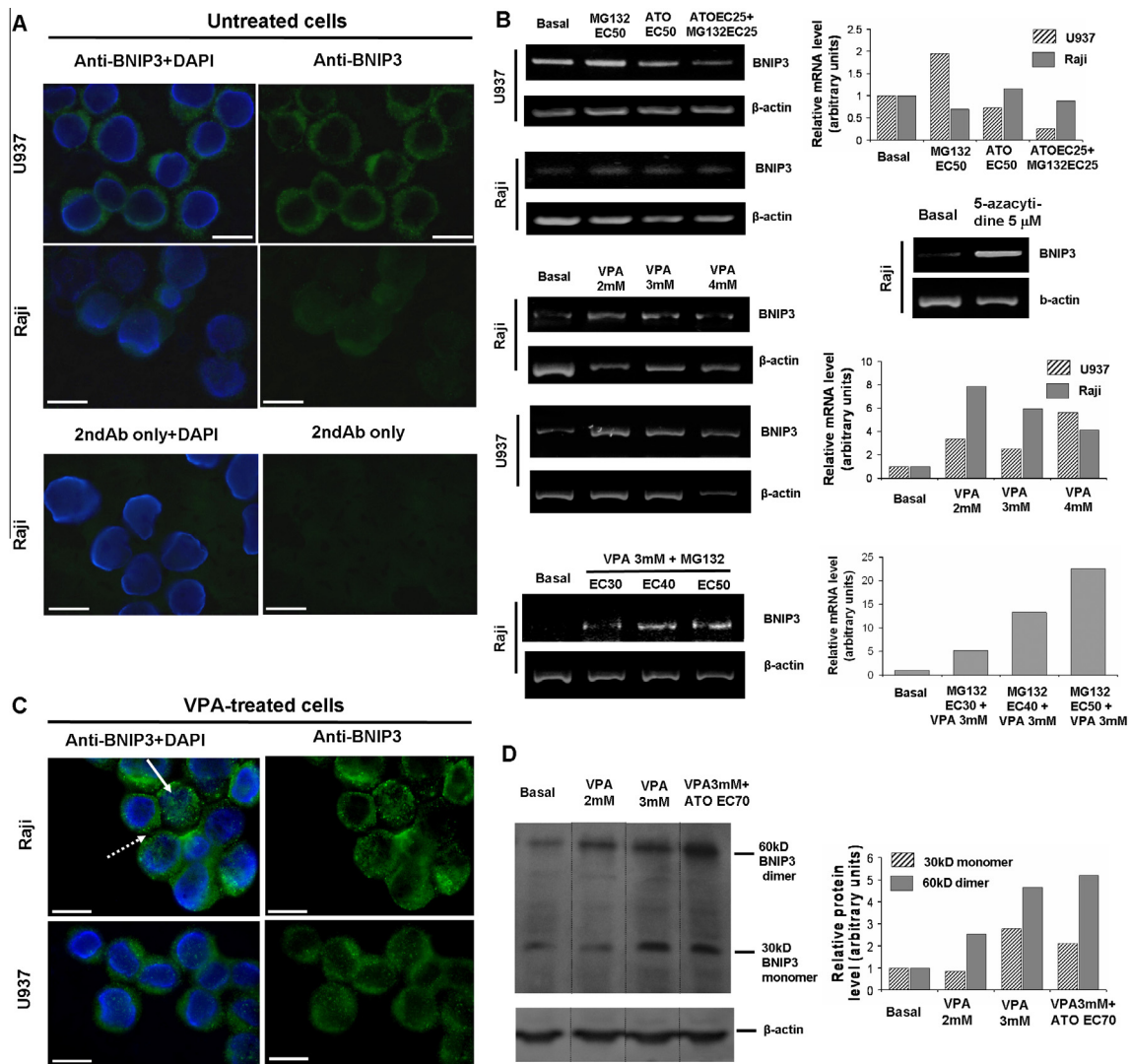
Fig. 3. Differential expression of BNIP3 in U937 and Raji cells. (A) Immunofluorescence detection of BNIP3 using a primary anti-BNIP3 Ab and a FITC-conjugated secondary Ab. Anti-BNIP3 + 4′,6-diamidino-2-phenylindole (DAPI) refers to digital overlay of a green fluorescent image with the DAPI fluorescence image of the same field to appreciate the relative distribution of BNIP3 around cytoplasmic and nuclear areas. Non-specific fluorescence detected by FITC-conjugated secondary antibody in Raji cells without primary anti-BNIP3 is also shown. Expression of BNIP3 in untreated Raji cells was slightly above non-specific fluorescence. Size bar = 10 μm. (B) Differential expression of BNIP3 mRNA evaluated by conventional RT-PCR of the 317 bp product in basal and drug-treated U937 and Raji cells. The corresponding μM values of EC% doses are shown in Table 1. β-actin served as an internal control for the integrity of the cDNA. Bar graphs indicate the corresponding densitometry values obtained. BNIP3 mRNA was upregulated by 5 μM-azacytidine and 2–4 mM valproic acid (VPA) in Raji cells, while MG132 increased BNIP3 mRNA in the presence of 3 mM VPA. (C) Raji cells treated with 3 mM VPA for 24 h and labelled with anti-BNIP3 showed increased fluorescence. Digitally overlaid DAPI-fluorescence image shows that cellular distribution of upregulated BNIP3 often included the central nuclear areas (white arrow), while adjacent cells kept marginal areas free of fluorescent label (dotted line arrow showing dark spaces between adjacent cells). VPA-treated U937 cells continued to show a peripheral cytoplasmic distribution of BNIP3 separated from the nuclear area. Size bar = 10 μm. (D) Western blot confirmed a dose dependent increase of 60 kDa dimer and 30 kDa monomer of BNIP3 protein in VPA-treated Raji cells. Lanes correspond to the same membrane. The lanes omitted in between indicated by the dotted lines correspond to the same evaluation in nuclear fractions. The complete image is shown in Supplementary Fig. S5.

cytometry) spanning a dose range of VPA to obtain the parameters of a dose–effect equation by the median effect method [8]. The resulting EC50 doses of VPA at 72 h were 6.22 mM and 4.20 mM for Raji cells and U937 cells respectively (Fig. 4A). In addition, we observed that VPA had no cytotoxic effect in Raji cells over the range 1–3 mM and increased autophagy within the range 2–4 mM, as indicated by percentage of MDC-positive cells scored by UV-excited flow cytometry

(Fig. 4B). By contrast, autophagy was suppressed within the cytotoxic dose range (Fig. 4B).

3.5. VPA did not sensitise Raji cells to ATO + MG132 cytotoxicity

Our first hypothesis was that subcytotoxic doses of VPA would act epigenetically to upregulate BNIP3 in Raji cells and would cause ATO to synergise with
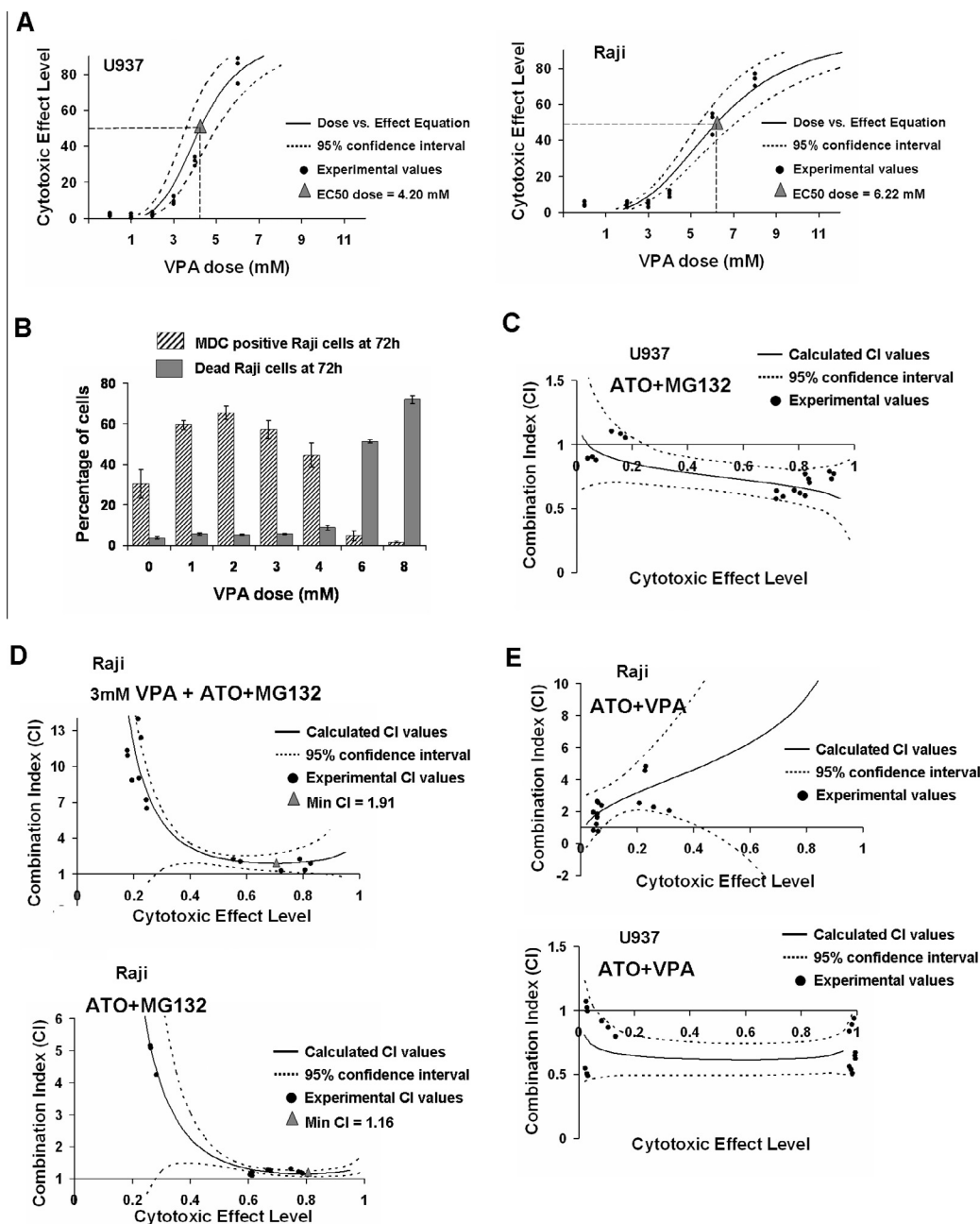
Fig. 4. The influence of VPA on the cytotoxic efficacy of arsenic trioxide (ATO) and MG132. (A) Plot of the dose–effect equation and EC50 calculation for valproic acid (VPA) in Raji and U937 cells. (B) Evaluation of autophagy (hatched bars) and cell death (grey bars) in Raji cells treated with increasing doses of VPA and evaluated at 72 h. Samples were assayed in triplicate and error bars indicate ±SD of the mean value. (C) Combination index (CI) function plot versus 72 h cytotoxic effect level showing synergism between ATO and MG132 in U937 cells (fixed ratio 4:1). (D) Combination index as a function of 72 h cytotoxic effect level corresponding to Raji cells treated with spanning doses of ATO + MG132 (fixed ratio 4:1) in the presence of 3 mM VPA (top graph) or without VPA (bottom graph). (E) CI function plot showing that VPA and ATO (fixed ratio 600:1) were exceedingly antagonistic in Raji cells (top graph), and strongly synergistic in U937 cells (bottom graph).

MG132 over the cell death effect as we have previously observed in U937 cells (Table 1 and Fig. 4C) [9]. However this hypothesis proved to be wrong in this case since the combination ATO + MG132 in the presence of sublethal 3 mM VPA was still antagonistic over the whole effect range (Fig. 4D). In fact, antagonism was increased from a lower bound of CI > 1.16 attained at EC80% to a lower bound of CI > 1.91 attained at EC70%. In

addition, we found that VPA and ATO were synergic in U937 cells but exceedingly antagonistic in Raji cells, since VPA treatment almost abolished ATO-induced cytotoxicity (Fig. 4E). Thus, constitutive down-regulation of BNIP3 could not explain the antagonistic interaction of ATO and MG132 in Raji cells. This remarkable increase of antagonism indicates that the potency of single drugs was strongly depreciated when
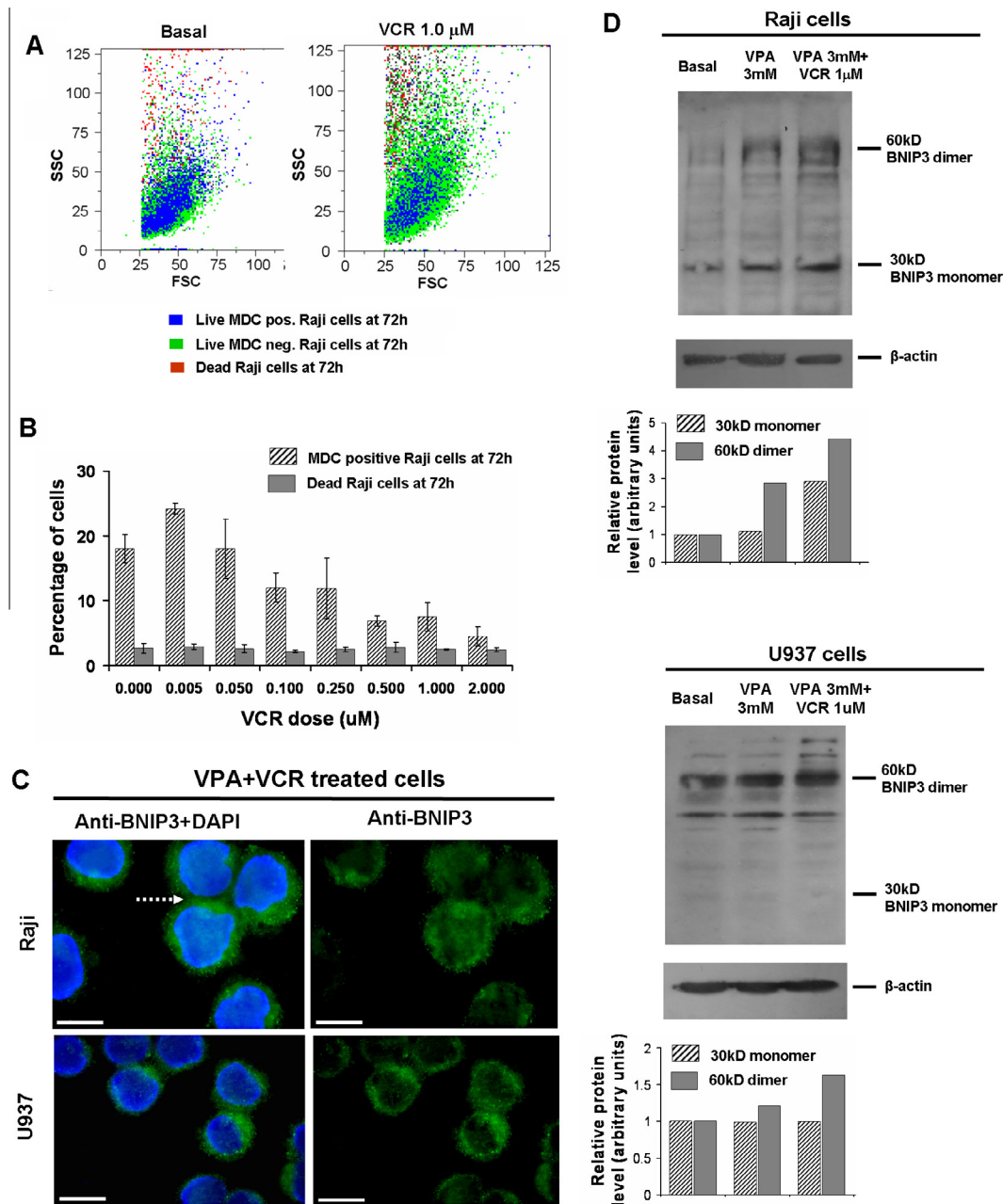
Fig. 5. The cellular distribution of valproic acid (VPA)-induced BNIP3 is modified by vincristine (VCR) treatment in Raji cells. (A) Representative dot plots corresponding to three colour flow cytometry of VCR-treated cells conducted to assess autophagy and cell death at 72 h. (B) Assessment of cytotoxicity of VCR at 72 h spanning doses from 5 nM to 2 μM. No cytotoxic effect was observed, and autophagy was blocked within the higher dose range (0.5 μM–2 μM). Samples were assayed in triplicate and error bars indicate ±SD of the mean value. (C) Immunofluorescence detection of BNIP3 in Raji and U937 cells treated with 3 mM VPA and 1 μM VCR for 24 h. Cellular distribution of BNIP3 changed to more marginal cytoplasmic locations in Raji cells. Fluorescent label often included marginal edges in adjacent cells (doted line arrow showing there are no dark spaces between adjacent cells). Distribution of BNIP3 in U937 cells showed no changes as compared to VPA-treatment alone (show in Fig. 3C). Size bar = 10 μm. (D) Western blot showing increased BNIP3 protein expression in cells treated with 3 mM VPA + 1 μM VCR particularly in Raji cells but also in U937 cells.

added in combination. Apart from the formal calculation of the CI index this lack of potency can be illustrated straightforward through the very low levels of cytotoxicity obtained at the experimental dose–effect values used to calculate the CI (shown in black dots in Fig. 4E). Some of these values are shown re-plotted as a dose–effect bar graph in Supplementary Fig. S6.

3.6. VCR inhibits autophagy in Raji cells at 72h without having any effect on cell viability

VCR had no cytotoxic effect at 72 h in Raji cells within the range 0.005 μM to 2 μM (Fig. 5A and B). In addition, VCR at doses above 0.5 μM almost abolished autophagy in Raji cells evaluated at 72 h, probably

owing to the long-term complete blockage of autophagic flow (Fig. 5A and B).

Viability in VCR-treated cells remained as high as untreated cells even though autophagy was completely abolished. This result demonstrates that autophagy itself does not provide a cell survival response because chemical inhibition of autophagy attained by VCR treatment had no effect on cell death. Cells treated for 24 h with VPA 3 mM + VCR 1 μM and analysed by fluorescence microscopy showed a redistribution of MDC-stained autophagosomes and AO stained lysosomes apart from the nuclear area and towards the cell edges (Supplementary Fig. S4). At 72 h Raji cells treated with VPA 3 mM + VCR 1 μM showed no MDC-stained autophagosomes through fluorescence microscopy but lysosomes were still detected by AO stain in accordance with inhibition of autophagy detected by flow cytometry (Supplementary Fig. S4). A comparable chemical inhibition of autophagy was attained with 10 mM 3MA in just 4 h as detected by flow cytometry of MDC-stained cells in agreement with 3MA inhibiting the formation of autophagosomes without having any effect on cell viability (Supplementary Fig. S7). Chemical inhibition of 3MA for 24 h and 72 h had no effect in cell viability as was the case with chemical inhibition with 1uM VCR (Supplementary Fig. S7).

3.7. VPA and VCR co-treatment changed the cellular location of BNIP3 in Raji cells

When Raji cells were exposed simultaneously to subcytotoxic doses of VPA and VCR (3 mM and 1 μM, respectively) for 24 h, and further stained for BNIP3 protein by immunofluorescence, the cellular distribution shifted from a predominantly perinuclear location to a distribution all over the cytoplasm, including the most peripheral areas and cell edges (Fig. 5C). Thus it resembled the cellular distribution of BNIP3 that we observed in untreated U937 cells, 3 mM VPA-treated U937 cells and even 3 mM VPA + 1 μM VCR-treated U937 cells (Figs. 3A, C and 5C respectively).

3.8. VPA and VCR co-treatment changed cellular location of mitochondria and increased mitochondrial mass

When stained with MTKred Raji cells treated with 3 mM VPA still showed mitochondria clustered around the nuclear area (Fig. 6A). In addition, these 3 mM VPA-treated cells showed a smaller area of fluorescent mitochondria than untreated cells (Fig. 6B). However, treating Raji cells with a combination of 3 mM VPA + 1 μM VCR caused a distribution of mitochondria apart from the nucleus and all around the cytoplasm, even approaching the edges defined by the cell membrane (Fig. 6A). This distribution of mitochondria

observed in Raji cells resembled that of untreated U937 cells, 3 mM VPA-treated U937 cells, and 3 mM VPA + 1 μM VCR-treated U937 cells (Figs. 3A, 3C and 6A). In addition the area of fluorescent mitochondria in Raji cells treated with 3 mM VPA + 1 μM VCR was increased (Fig. 6B). The area of fluorescent mitochondria was not modified in U937 cells by 3 mM VPA but was increased by 3 mM VPA + 1 μM VCR (Fig. 6B).

Mitochondrial mass was increased in Raji and U937 cells by VPA and even more by VPA + VCR as detected by NAO probe and flow cytometry (Supplementary Fig. S8). When cells were stained with both MDC and MTKred and analysed by fluorescence microscopy, the colocalisation between the two fluorophores was increased in samples treated with 3 mM VPA + 1 μM VCR as compared to 3 mM VPA alone (Supplementary Fig. S9). When simultaneously stained with MTKred and anti-BNIP3 Raji cells treated with VPA or VPA + VCR showed colocalisation of mitochondria and BNIP3 label and the same resulted for untreated and VPA-treated U937 cells (Supplementary Fig. S10). Changes in autophagosome abundance and distribution caused by VPA and VPA + VCR were also noted in Raji cells transfected with pRFP-LC3. Treatment with 3 mM VPA caused dot-like fluorescent patterns, particularly in areas around the nucleus, which colocalised with MDC fluorescence. Treatment with 3 mM VPA + 1 μM VCR caused fluorescent dots to distribute more towards the cell edges (Supplementary Fig. S11).

3.9. VPA and VCR co-treatment sensitised Raji cells to a loss of MMP inflicted by ATO+MG132

We next evaluated again the changes in MMP occurring at 24 h with doses of ATO and MG132 known to cause cytotoxicity at 72 h but now with 3 mM VPA and 1 μM VCR. In the presence of 3 mM VPA alone Raji cells treated with ATO EC50, MG132 EC50 and ATO EC25 + MG132 EC25, the percentage of cells with collapsed MMP was low and comparable to that of treatments without 3 mM VPA (shown in Fig. 1B), while MMP was kept high in the remaining cells, and even above the basal level in the case of MG132 EC50 (Fig. 7A). However, in the presence of both 3 mM VPA and 1 μM VCR all three treatments ATO EC50, MG132 EC50, and ATO EC25 + MG132 EC25 increased the percentage of cells with collapsed MMP, and lowered the potential in those cells that still kept a positive MMP (Fig. 7A).

3.10. MG132 and ATO were synergic in Raji cells treated with subcytotoxic VPA+VCR

We finally assessed the combination ATO + MG132 at doses spanning the whole cytotoxic effect range in Raji cells in the presence of 3 mM VPA and 1 μM VCR. Under this condition the combination
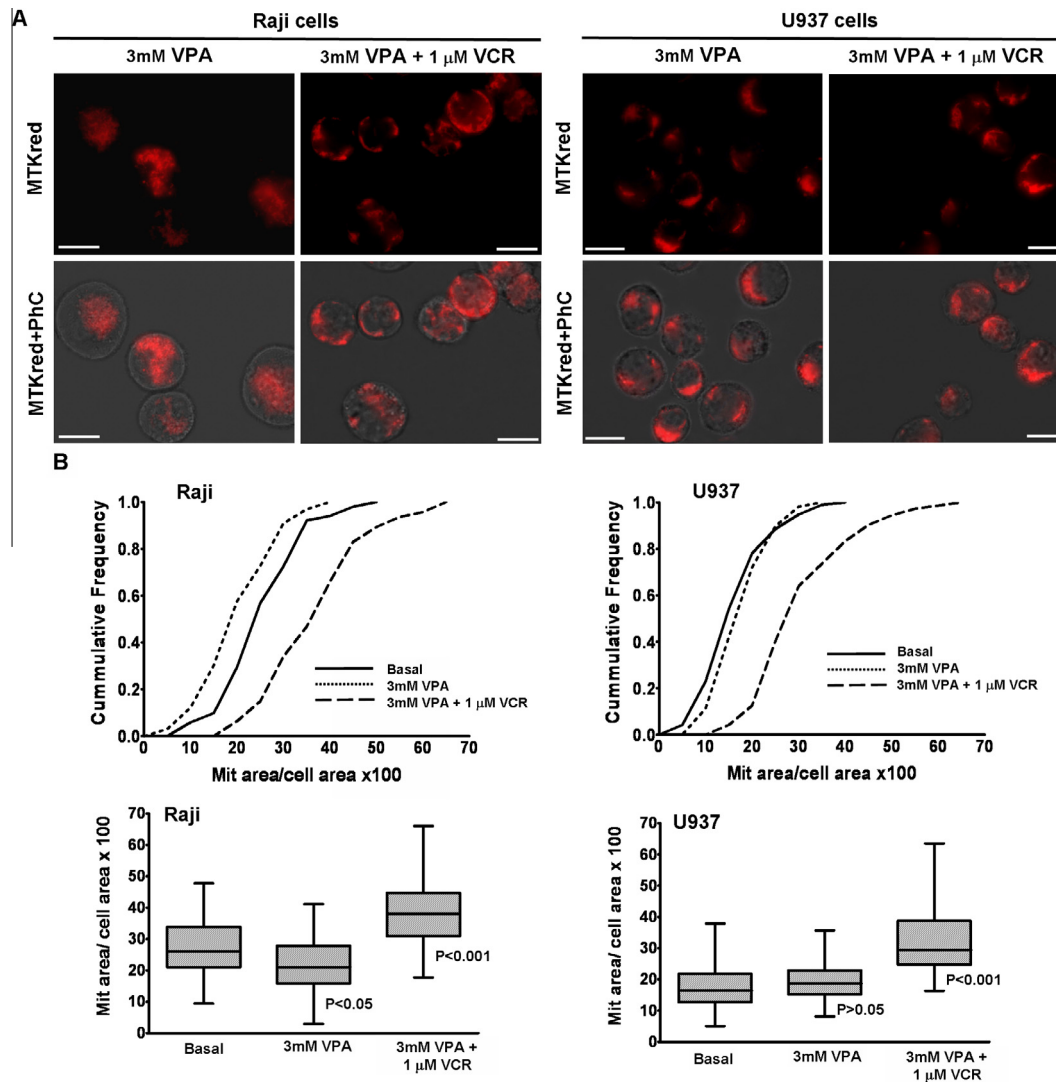
Fig. 6. The cellular distribution of mitochondria is modified by vincristine (VCR) treatment in Raji cells but not in U937 cells. (A) Cellular distribution of mitochondria in cells treated with 3 mM valproic acid (VPA) alone or 3 mM VPA + 1 μM VCR after 24 h. Distribution of mitochondria changed with 3 mM VPA + 1 μM VCR (but not with VPA alone) from central location over the nucleus to a peripheral cytoplasmic location. Size bar = 10 μm. (B) 3 mM VPA + 1 μM VCR treatment increased mitochondrial mass in both cell lines, while 3 mM VPA alone reduced slightly the mitochondrial mass in Raji cells. Data were obtained as previously described in Fig. 1. Box–Whisker plots show median, quartiles, and extreme values together with the level of significance of the *p*-value in Tukey–Kramer's post test for differences between treatment and basal (following a significant ANOVA test with $p < 0.001$).

ATO + MG132 shifted from an antagonistic kind of interaction to a synergistic one particularly at mid to high effect doses (CI < 1 attained at effects levels above EC50) resembling the results previously achieved in U937 cells (Fig. 7B, Fig. 4C). By contrast, the combination ATO + MG132 was still antagonistic when only 1 μM VCR was present, achieving a lower bound of CI > 1.09 at EC75% (Supplementary Fig. S12). Neither ATO + MG132 + 1 μM VCR nor 1 μM VCR alone upregulated BNIP 3mRNA (Supplementary Fig. S12b).

4. Discussion

The aim of this study was to target potential mechanisms of resistance to the combination of ATO with

MG132 in Raji cells in order to completely change the kind of interaction of these two cytotoxic drugs from antagonism to synergism.

MG132 is a peptide aldehyde that inhibits mainly chemotrypsin-like activity of the 26S proteasome by covalently binding to the active site of the β5 subunit [30–32]. MG132 has the same target as Bortezomib and new generation proteasome inhibitors. Mutations in the highly conserved Bortezomib pocket binding of β5 subunit cause cross-resistance with MG132 [33]. Another cause of resistance to Bortezomib, MG132 and new generations of proteasome inhibitors is the presence of alternate methods of protein degradation such as autophagy [34]. The ubiquitin proteasome system and autophagy may be functionally coupled since
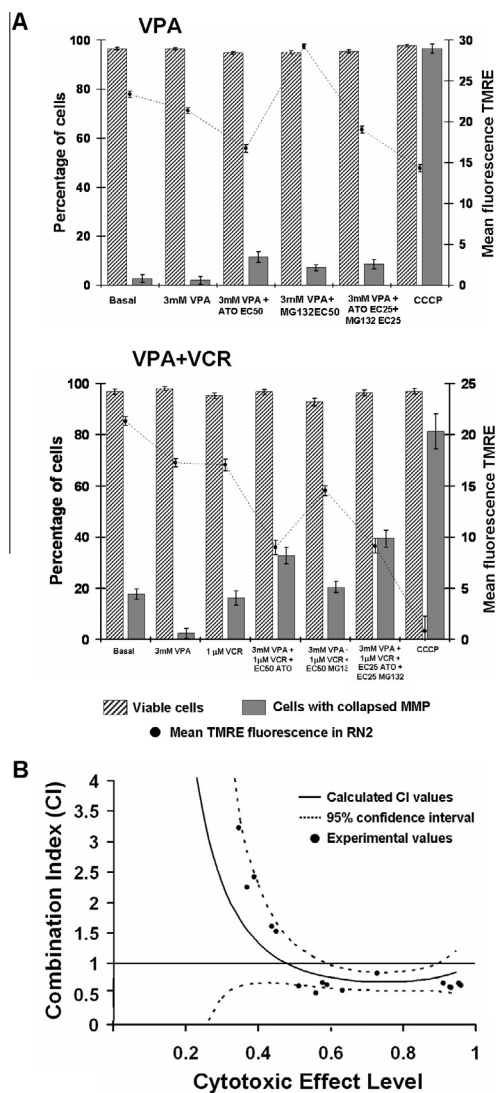
Fig. 7. Synergism between arsenic trioxide (ATO) and MG132 in Raji cells with low doses of valproic acid (VPA) and vincristine (VCR). (A) The top graph (VPA) shows that a subcytotoxic dose of 3 mM VPA alone in Raji cells had no sensitising effect on mitochondrial membrane potential (MMP) collapse or low MMP. The graph below (VPA + VCR) shows that the addition of 3 mM VPA together with 1 μM VCR had a strong sensitising effect increasing the percentage of cells with collapsed MMP and causing decreased mean TMRE fluorescence, particularly with ATO EC50 and ATO EC25 + MG132 EC25 (RN2 refers to the region of cells with polarised mitochondria as illustrated in Fig. 1A). The percentage of viable cells as detected by exclusion of the non-permeable dye DAPI is shown in hatched bars (left axis) Samples were assayed in triplicate and error bars indicate ±SD of the mean value. (B) Combinatory index (CI) as a function of cytotoxic effect level (dark line) with 95% confidence level intervals (dotted lines) and experimental values (black dots) showing that ATO + MG132 (fixed molar ratio 4:1) became a synergic combination (CI < 1) in the presence of subcytotoxic doses of 3 mM VPA and 1 μM VCR.

proteasome inhibition activates autophagy and suppression of autophagy promotes the accumulation of poly-ubiquitinated protein aggregates.[35]. ATO is known to target the mitochondria, increasing intracellular ROS, and triggering intrinsic apoptosis [3,4]. In several models it was shown that ATO induces autophagy,

and inhibition of autophagy may result in reversal of effects on leukaemic cells [36,37]. Our study showed that the combination ATO + MG132 increased autophagy in U937 and Raji cells at 24 h using 72 h cytotoxic doses, while BNIP3 was found to be expressed constitutively in U937 cells but not in Raji cells. ATO has been shown to induce cell death through an autophagic mechanism mediated by BNIP3 in malignant glioma cells [23]. Hypoxia-induced cell death is also mediated by autophagy through BNIP3 in glioma and breast cancer cells [21], and a cDNA microarray analysis showed that ATO upregulates several genes involved in response to hypoxia [23]. It was suggested that ATO may induce a hypoxic status in tumour cells, where BNIP3 is subsequently upregulated, leading to autophagic cell death [23]. In agreement with our finding in U937 cells, BNIP3 is overexpressed in several types of cancer and is associated with poor prognosis [38–40].

By contrast we found that Raji cells had a very low expression of BNIP3 at the mRNA and protein levels. Downregulation of BNIP3 may result in a failure of tumour cells to undergo cell death and is associated with a chemoresistant phenotype and decreased patient survival [41–43]. Samples from patients with multiple myeloma were found methylated at the BNIP3 promoter and methylation was significantly correlated with poor patient survival rates [44]. Our results showed that HDAC inhibitor VPA upregulated BNIP3 in Raji cells. Silencing BNIP3 expression was proposed to be selected for by cancer cells to evade death signals induced by hypoxia or chemotherapeutic drugs [14,41,45]. Having found that ATO + MG132 increased autophagy in both cell lines and that BNIP3 was expressed in U937 cells, we assumed that resistance of Raji cells to ATO + MG132 could reside in the epigenetic silencing of BNIP3. Thus we thought that the addition of a VPA dose, high enough to upregulate BNIP3 but still without any cytotoxic effect, would enable the pro-death role of BNIP3 to be triggered by ATO + MG132 and the pharmacological interaction would turn into synergism. However the strong antagonism that we observed between ATO and MG132 in the presence of low doses of VPA led us to consider that upregulation of BNIP3 in Raji cells was exerting a protective role against ATO. A previous study found that autophagy protected against BNIP3-mediated cell death in HL-1 cells [46], while BNIP3-induced autophagy during hypoxia was demonstrated as a survival mechanism in several tumour cell lines [47]. The death function of BNIP3 in a hypoxic tumour environment was questioned in other studies finding that rapid and full induction of BNIP3 could instead protect from cell death through an autophagic process [17]. Moreover, it was proposed that BNIP3 is a pro-autophagic protein with a strictly pro-survival role that is required for the optimal induction of autophagy in hypoxia [16].

In our study we noted that BNIP3 distribution in VPA-treated Raji cells was restricted to nuclear and perinuclear areas. This was in clear contrast to the distribution of BNIP3 and mitochondria in U937 cells. It was previously shown that nuclear localisation of BNIP3 negates its pro-cell death function [48].

Our study showed that 72 h cytotoxic doses of ATO and MG132 had no effect on MMP at 24 h in Raji cells, contrasting the effect that they had in U937 cells.

Moreover, single treatment with VPA upregulated BNIP3, while MG132 only in the presence of VPA contributed to upregulate BNIP3 mRNA in Raji cells, yet VPA treatment caused no change over basal MMP or even increased MMP over basal levels when combined with MG132 as shown in Fig. 7. However, most studies coincide in that BNIP3 is primarily localised to the mitochondria, and induces loss of MMP and cell death [49–51]. And in fact this was consistent with our results in constitutive BNIP3-positive U937 cells but not with VPA-treated BNIP3-positve Raji cells.

Recent studies have shown that fragmented mitochondria with low MMP aggregate in the perinuclear region where they are removed by selective autophagy [19,20,52]. Selective removal of mitochondria by autophagy, often called mitophagy may occur independently of general autophagy to specifically remove damaged or excessive organelles and even under nutrient-rich conditions [53].

Transport of mitochondria to the perinuclear region for elimination is dependent on the microtubule network and treatment of cells with microtubule destabilising agents inhibits perinuclear mitochondrial aggregation and mitophagy [19,20]. It was suggested that transport of mitochondria via the microtubules to the perinuclear region is an essential step in the mitochondrial degradation pathway [12]. VCR as other vinca alkaloids also blocks the fusion of autophagosomes and lysosomes thus halting autophagic flux [29]. The treatment with VCR changed the cellular distribution of VPA-induced BNIP3 and mitochondria. In addition autophagosomes colocalised with mitochondria, while mitochondrial mass was increased and MMP was decreased. So we conclude that VCR caused a blockage of mitophagic flux and an accumulation of damaged mitochondria [13,54]. At this point our results had been partially reconciled with the paradigm stating that BNIP3 induces loss of MMP and cell death [49–51].

The complete reconciliation with the paradigm stating that BNIP3 induces mitochondrial dysfunction and cell death [49–51] came only after finding that the kind of interaction between ATO and MG132 shifted from antagonism (CI > 1) to synergism (CI < 1) in the presence of a low dose of VPA that upregulated BNIP3, and a low dose of VCR that blocked mitophagic flux. Antagonism between ATO + MG132 was not modified by adding only a low dose of VCR where BNIP3 was not upregulated. So the requirement for BNIP3 to exert its pro-death effect in Raji cells could be its sustained location at the mitochondria through blockage of mitophagic flux. The persistence of this situation would lead to an increasing load of damaged mitochondria. However our results are also in agreement with BNIP3 being part of a pro-survival resistance mechanism that eliminates mitochondria through mitophagy [55,56] and contributes to reduce the potential stress that outcomes from damaged mitochondria. Thus, shifting the kind of cytotoxic interaction between ATO and MG132 from antagonism to synergism in Raji cells required overcoming a resistance system that involved BNIP3, the microtubule transport network and selective autophagy of mitochondria (mitophagy).

Our main conclusion is that reverting epigenetic silencing of BNIP3 can result in improved mitophagy and increased tolerance to mitochondrial damage thus lowering the efficacy of drugs that target the mitochondria, increase ROS and reduce MMP as is the case of ATO. Under this situation epigenetic drugs will increase tumour cell survival. However, this system depends heavily on the microtubule network to transport and eliminate mitochondria, and microtubule destabilising agents will block mitophagy.

The resistance system we describe in this study may not be restricted to Burkitt's lymphoma cells but may appear in several types of tumour cells. Moreover, it could be present in some patients and absent in others with a same disease and may explain differences in treatment response outcome. In Fig. S15 we show results from a combination analysis identical to the one presented in this study conducted in pathological cells obtained from peripheral blood of a patient diagnosed with adult T-cell leukaemia-lymphoma associated to HTLV-1 infection that was in best supportive care for several weeks after a poor response to Peg-Interferon alpha-2b. The analysis showed that ATO + MG132 was antagonistic but could be turned into synergism by low doses of VPA and VCR. In cells from this particular patient the EC50 of ATO and MG132 was reduced more than 10 times in the presence of VPA + VCR (Fig. S15).

In a second case shown in Fig. S16, ATO and VPA were evaluated in circulating blast cells obtained from a patient diagnosed with acute myeloid leukaemia corresponding to M6 FAB classification (erythroleukaemia). The combined drugs were synergic as was the case in promonocytic cell line U937 shown in Fig. 4E. The addition of 1 μM VCR as single drug did not induce cytotoxicity above basal levels but increased synergism when added to combined ATO + VPA (Fig. S16).

Our findings may have potential contributions to hypomethylating and HDAC based therapies. At present, the mechanism of resistance and failure to hypomethylating agents either as single agents or combined with

HDACs is not understood and it is difficult to develop targeted interventions for these patients. In addition there are no predictors of response to hypomethylating drugs [57]. Our study introduces the concept that increased mitophagic flux is a possible explanation to failure of hypomethylating and HDAC based therapies. Similarly, our results suggest that in some cases increased mitophagic flux can explain resistance to proteasome inhibitors [58]. In addition our study introduces several potential biomarkers of effect that could become predictors of response. These biomarkers include the kind of interaction between ATO and a proteasome inhibitor over cytotoxic effect, changes in BNIP3 expression induced by epigenetic drugs, basal mitophagic flux and changes in mitophagic flux induced by drugs such as VCR and VPA together with its impact on MMP and intracellular ROS production. All these biomarkers can be evaluated in xenograft animal models and tumour cells obtained from patients.

Conflict of interest statement

None declared.

Acknowledgements

Appendix A. Supplementary data

Supplementary data associated with this article can be found, in the online version, at http://dx.doi.org/10.1016/j.ejca.2014.09.012.

References

[1] Hu J, Liu YF, Wu CF, Xu F, Shen ZX, Zhu YM, et al. Long-term efficacy and safety of all-trans retinoic acid/arsenic trioxide-based therapy in newly diagnosed acute promyelocytic leukemia. Proc Natl Acad Sci U S A 2009;106(9):3342–7.

[2] Platanias LC. Biological responses to arsenic compounds. J Biol Chem 2009;284(28):18583–7.

[3] Emadi A, Gore SD. Arsenic trioxide – An old drug rediscovered. Blood Rev 2010;24(4–5):191–9.

[4] Li L, Wang J, Ye RD, Shi G, Jin H, Tang X, et al. PML/RARalpha fusion protein mediates the unique sensitivity to arsenic cytotoxicity in acute promyelocytic leukemia cells: Mechanisms involve the impairment of cAMP signaling and the aberrant regulation of NADPH oxidase. J Cell Physiol 2008;217(2):486–93.

[5] Ito K, Bernardi R, Morotti A, Matsuoka S, Saglio G, Ikeda Y, et al. PML targeting eradicates quiescent leukaemia-initiating cells. Nature 2008;453(7198):1072–8.

[6] Chanan-Khan AA, Borrello I, Lee KP, Reece DE. Development of target-specific treatments in multiple myeloma. Br J Haematol 2010;151(1):3–15.

[7] Chou TC. Drug combination studies and their synergy quantification using the Chou–Talalay method. Cancer Res 2010;70(2):440–6.

[8] Lombardo T, Anaya L, Kornblihtt L, Blanco G. Median effect dose and combination index analysis of cytotoxic drugs using flow cytometry. Rijeka, Croatia: Intech Open Publisher; 2012.

[9] Lombardo T, Cavaliere V, Costantino SN, Kornblihtt L, Alvarez EM, Blanco GA. Synergism between arsenite and proteasome inhibitor MG132 over cell death in myeloid leukaemic cells U937 and the induction of low levels of intracellular superoxide anion. Toxicol Appl Pharmacol 2011;258(3):351–66.

[10] Al-Mehdi AB, Pastukh VM, Swiger BM, Reed DJ, Patel MR, Bardwell GC, et al. Perinuclear mitochondrial clustering creates an oxidant-rich nuclear domain required for hypoxia-induced transcription. Sci Signal 2010;5(231):ra47.

[11] Mellor HR, Harris AL. The role of the hypoxia-inducible BH3-only proteins BNIP3 and BNIP3L in cancer. Cancer Metastasis Rev 2007;26(3–4):553–66.

[12] Gottlieb RA, Gustafsson AB. Mitochondrial turnover in the heart. Biochim Biophys Acta 2011;1813(7):1295–301.

[13] Hanna RA, Quinsay MN, Orogo AM, Giang K, Rikka S, Gustafsson AB. Microtubule-associated protein 1 light chain 3 (LC3) interacts with Bnip3 protein to selectively remove endoplasmic reticulum and mitochondria via autophagy. J Biol Chem 2012;287(23):19094–104.

[14] Burton TR, Gibson SB. The role of Bcl-2 family member BNIP3 in cell death and disease: NIPping at the heels of cell death. Cell Death Differ 2009;16(4):515–23.

[15] Zhang L, Li L, Liu H, Prabhakaran K, Zhang X, Borowitz JL, et al. HIF-1alpha activation by a redox-sensitive pathway mediates cyanide-induced BNIP3 upregulation and mitochondrial-dependent cell death. Free Radic Biol Med 2007;43(1):117–27.

[16] Mazure NM, Pouyssegur J. Atypical BH3-domains of BNIP3 and BNIP3L lead to autophagy in hypoxia. Autophagy 2009;5(6):868–9.

[17] Pouyssegur J, Dayan F, Mazure NM. Hypoxia signalling in cancer and approaches to enforce tumour regression. Nature 2006;441(7092):437–43.

[18] Okatsu K, Saisho K, Shimanuki M, Nakada K, Shitara H, Sou YS, et al. P62/SQSTM1 cooperates with Parkin for perinuclear clustering of depolarized mitochondria. Genes Cells 2010;15(8):887–900.

[19] Vives-Bauza C, Zhou C, Huang Y, Cui M, de Vries RL, Kim J, et al. PINK1-dependent recruitment of Parkin to mitochondria in mitophagy. Proc Natl Acad Sci U S A 2010;107(1):378–83.

[20] Lee JY, Nagano Y, Taylor JP, Lim KL, Yao TP. Disease-causing mutations in parkin impair mitochondrial ubiquitination, aggregation, and HDAC6-dependent mitophagy. J Cell Biol 2010;189(4):671–9.

[21] Azad MB, Chen Y, Henson ES, Cizeau J, McMillan-Ward E, Israels SJ, et al. Hypoxia induces autophagic cell death in apoptosis-competent cells through a mechanism involving BNIP3. Autophagy 2008;4(2):195–204.

[22] Bristow N, Burton TR, Henson ES, Ong-Justiniano C, Brown M, Gibson SB. Truncated forms of BNIP3 act as dominant negatives inhibiting hypoxia-induced cell death. Biochim Biophys Acta 2011;1812(3):302–11.

[23] Kanzawa T, Zhang L, Xiao L, Germano IM, Kondo Y, Kondo S. Arsenic trioxide induces autophagic cell death in malignant glioma cells by upregulation of mitochondrial cell death protein BNIP3. Oncogene 2005;24(6):980–91.

[24] Murai M, Toyota M, Satoh A, Suzuki H, Akino K, Mita H, et al. Aberrant DNA methylation associated with silencing BNIP3 gene expression in haematopoietic tumours. Br J Cancer 2005;92(6):1165–72.

[25] Cavaliere V, Papademetrio DL, Lombardo T, Costantino SN, Blanco GA, Alvarez EM. Caffeic acid phenylethyl ester and MG132, two novel nonconventional chemotherapeutic agents, induce apoptosis of human leukemic cells by disrupting mitochondrial function. Target Oncol 2013.

[26] Cavaliere V, Papademetrio DL, Alvarez EM, Blanco GA. Haemostatic and immune role of cellular clotting in the sipunculan Themiste petricola. Cell Tissue Res 2010;339(3):597–611.

[27] Cordo Russo RI, Garcia MG, Alaniz L, Blanco G, Alvarez E, Hajos SE. Hyaluronan oligosaccharides sensitize lymphoma resistant cell lines to vincristine by modulating P-glycoprotein activity and PI3K/Akt pathway. Int J Cancer 2008;122(5): 1012–8.

[28] Semenza GL. Hypoxia-inducible factor 1: regulator of mitochondrial metabolism and mediator of ischemic preconditioning. Biochim Biophys Acta 2011;1813(7):1263–8.

[29] Munafo DB, Colombo MI. A novel assay to study autophagy: regulation of autophagosome vacuole size by amino acid deprivation. J Cell Sci 2001;114(Pt 20):3619–29.

[30] Lee DH, Goldberg AL. Proteasome inhibitors: valuable new tools for cell biologists. Trends Cell Biol 1998;8(10):397–403.

[31] Kloss A, Meiners S, Ludwig A, Dahlmann B. Multiple cardiac proteasome subtypes differ in their susceptibility to proteasome inhibitors. Cardiovasc Res 2013;85(2):367–75.

[32] Han YH, Moon HJ, You BR, Park WH. The effect of MG132, a proteasome inhibitor on HeLa cells in relation to cell growth, reactive oxygen species and GSH. Oncol Rep 2009;22(1): 215–21.

[33] Oerlemans R, Franke NE, Assaraf YG, Cloos J, van Zantwijk I, Berkers CR, et al. Molecular basis of bortezomib resistance: proteasome subunit beta5 (PSMB5) gene mutation and overexpression of PSMB5 protein. Blood 2008;112(6):2489–99.

[34] Kumar S, Rajkumar SV. Many facets of bortezomib resistance/susceptibility. Blood 2008;112(6):2177–8.

[35] Ding WX, Ni HM, Gao W, Yoshimori T, Stolz DB, Ron D, et al. Linking of autophagy to ubiquitin-proteasome system is important for the regulation of endoplasmic reticulum stress and cell viability. Am J Pathol 2007;171(2):513–24.

[36] Goussetis DJ, Altman JK, Glaser H, McNeer JL, Tallman MS, Platanias LC. Autophagy is a critical mechanism for the induction of the antileukemic effects of arsenic trioxide. J Biol Chem 2010;285(39):29989–97.

[37] Isakson P, Bjoras M, Boe SO, Simonsen A. Autophagy contributes to therapy-induced degradation of the PML/RARA oncoprotein. Blood 2010;116(13):2324–31.

[38] Giatromanolaki A, Koukourakis MI, Gatter KC, Harris AL, Sivridis E. BNIP3 expression in endometrial cancer relates to active hypoxia inducible factor 1alpha pathway and prognosis. J Clin Pathol 2008;61(2):217–20.

[39] Sowter HM, Ferguson M, Pym C, Watson P, Fox SB, Han C, et al. Expression of the cell death genes BNip3 and NIX in ductal carcinoma in situ of the breast; correlation of BNip3 levels with necrosis and grade. J Pathol 2003;201(4):573–80.

[40] Leo C, Horn LC, Hockel M. Hypoxia and expression of the proapoptotic regulator BNIP3 in cervical cancer. Int J Gynecol Cancer 2006;16(3):1314–20.

[41] Okami J, Simeone DM, Logsdon CD. Silencing of the hypoxia-inducible cell death protein BNIP3 in pancreatic cancer. Cancer Res 2004;64(15):5338–46.

[42] Erkan M, Kleeff J, Esposito I, Giese T, Ketterer K, Buchler MW, et al. Loss of BNIP3 expression is a late event in pancreatic cancer contributing to chemoresistance and worsened prognosis. Oncogene 2005;24(27):4421–32.

[43] Murai M, Toyota M, Suzuki H, Satoh A, Sasaki Y, Akino K, et al. Aberrant methylation and silencing of the BNIP3 gene in colorectal and gastric cancer. Clin Cancer Res 2005;11(3):1021–7.

[44] Heller G, Schmidt WM, Ziegler B, Holzer S, Mullauer L, Bilban M, et al. Genome-wide transcriptional response to 5-aza-2′-deoxycytidine and trichostatin a in multiple myeloma cells. Cancer Res 2008;68(1):44–54.

[45] Ishida M, Sunamura M, Furukawa T, Akada M, Fujimura H, Shibuya E, et al. Elucidation of the relationship of BNIP3 expression to gemcitabine chemosensitivity and prognosis. World J Gastroenterol 2007;13(34):4593–7.

[46] Hamacher-Brady A, Brady NR, Logue SE, Sayen MR, Jinno M, Kirshenbaum LA, et al. Response to myocardial ischemia/reperfusion injury involves Bnip3 and autophagy. Cell Death Differ 2007;14(1):146–57.

[47] Bellot G, Garcia-Medina R, Gounon P, Chiche J, Roux D, Pouyssegur J, et al. Hypoxia-induced autophagy is mediated through hypoxia-inducible factor induction of BNIP3 and BNIP3L via their BH3 domains. Mol Cell Biol 2009;29(10):2570–81.

[48] Burton TR, Henson ES, Baijal P, Eisenstat DD, Gibson SB. The pro-cell death Bcl-2 family member, BNIP3, is localized to the nucleus of human glial cells: Implications for glioblastoma multiforme tumor cell survival under hypoxia. Int J Cancer 2006;118(7):1660–9.

[49] Regula KM, Ens K, Kirshenbaum LA. Inducible expression of BNIP3 provokes mitochondrial defects and hypoxia-mediated cell death of ventricular myocytes. Circ Res 2002;91(3):226–31.

[50] Vande Velde C, Cizeau J, Dubik D, Alimonti J, Brown T, Israels S, et al. BNIP3 and genetic control of necrosis-like cell death through the mitochondrial permeability transition pore. Mol Cell Biol 2000;20(15):5454–68.

[51] Kubli DA, Ycaza JE, Gustafsson AB. Bnip3 mediates mitochondrial dysfunction and cell death through Bax and Bak. Biochem J 2007;405(3):407–15.

[52] Twig G, Elorza A, Molina AJ, Mohamed H, Wikstrom JD, Walzer G, et al. Fission and selective fusion govern mitochondrial segregation and elimination by autophagy. Embo J 2008;27(2):433–46.

[53] Ding WX, Yin XM. Mitophagy: mechanisms, pathophysiological roles, and analysis. Biol Chem 2012;393(7):547–64.

[54] Klionsky DJ, Abdalla FC, Abeliovich H, Abraham RT, Acevedo-Arozena A, Adeli K, et al. Guidelines for the use and interpretation of assays for monitoring autophagy. Autophagy 2012;8(4):445–544.

[55] Quinsay MN, Thomas RL, Lee Y, Gustafsson AB. Bnip3-mediated mitochondrial autophagy is independent of the mitochondrial permeability transition pore. Autophagy 2010;6(7):855–62.

[56] Rikka S, Quinsay MN, Thomas RL, Kubli DA, Zhang X, Murphy AN, et al. Bnip3 impairs mitochondrial bioenergetics and stimulates mitochondrial turnover. Cell Death Differ 2011;18(4):721–31.

[57] García-Manero G. Therapeutic modalities and new molecular targets in MDS. London, UK: Springer; 2011.

[58] Jia L, Gopinathan G, Sukumar JT, Gribben JG. Blocking autophagy prevents bortezomib-induced NF-kappaB activation by reducing I-kappaBalpha degradation in lymphoma cells. PLoS One 2012;7(2):e32584.